ELSEVIER

Dyes and Pigments 47 (2000) 207–218

DYES and PIGMENTS

www.elsevier.com/locate/dyepig

Advanced chemical oxidation of reactive dyes in simulated dyehouse effluents by ferrioxalate-Fenton/UV-A and TiO_2/UV-A processes

İdil Arslan [a], Işil Akmehmet Balcioğlu [a,*], Detlef W. Bahnemann [b]

[a] *Boğaziçi University Institute of Environmental Sciences, 80815 Bebek, Istanbul, Turkey*
[b] *Institut für Solarenergieforschung Hameln/Emmerthal ISFH, Aussenstelle Hanover, D-30165 Hanover, Germany*

Received 27 October 1999; received in revised form 29 January 2000; accepted 15 May 2000

Abstract

Effective degradation of various mono- and bifunctional aminochlorotriazine reactive dyes in simulated dyehouse wastewater was achieved by the application of ferrioxalate-photo-Fenton [$Fe(C_2O_4)_3^{3-}/H_2O_2$/UV-A; 300 nm > λ > 400 nm] and titanium dioxide-mediated heterogeneous photocatalytic (TiO_2/UV-A) treatment processes. These so-called advanced oxidation processes were studied in a novel batch photoreactor that was irradiated by a solar simulating installation. Decolorization by the ferrioxalate-photo-Fenton oxidation process was found to proceed three times faster than the photocatalytic process, while the latter was more efficient in reducing the optical density at 280 nm wavelength (UV_{280nm}). Complete decolourization and partial mineralization with 17–23% total organic carbon (TOC) and 73–86% UV_{280nm} removals were achieved by the ferrioxalate-Fenton/UV-A and TiO_2/UV-A processes, respectively, within a 1-h treatment time. Emphasis was placed on the effect of dyehouse effluent strength on decolourization kinetics, along with possible advantages of the ferrioxalate-Fenton/UV-A process over the conventional photo-Fenton (Fe^{2+}/H_2O_2/UV-C) process. The results of these experiments showed that the more dilute the dyehouse effluent the faster the decolourization rate. On the basis of spectrophotometric measurements, dye decomposition could be successfully fitted to the empirical Langmuir–Hinshelwood kinetic model.

Keywords: Simulated reactive dyebath effluent; Aminochlorotriazine dyes; Advanced oxidation processes; Heterogeneous photocatalytic treatment; Photo-Fenton's oxidation; Ferrioxalate-photo-Fenton reaction

1. Introduction

Colour removal from textile wastewater has been a matter of considerable interest during the last two decades, not only because of the potential toxicity of certain dyes but often due to their visibility in receiving waters. Recent studies indicated that approximately 12% of synthetic dyes is lost annually during manufacturing and processing operations and that 20% of the resultant color enter the environment through effluents from industrial wastewater treatment plants [1].

Colour in dyehouse effluents has often been associated with the application of reactive dye-

* Corresponding author. Tel.: +90-212-2631540; fax: +90-212-2575033.
E-mail address: balciogl@boun.edu.tr (I.A.Balcioğlu).

0143-7208/00/$ - see front matter
PII: S0143-7208(00)00082-6

stuffs, during which up to 50% of the dyes may be lost to the effluent [2]. Reactive dyes are present in a hydrolyzed state in the exhausted dyebath or wash-water, a form that can not be reused in the dyeing process. Moreover, their photolytical/chemical stability and extremely low physical affinity [3] for various adsorbents make conventional treatment a rather difficult task.

Almost 70% of all reactive dyes are of the azo type [2]. Most of these dyes are resistant to aerobic biotreatment [3,4], but they can be decolourized anaerobically via reductive cleavage of the –N=N– bonds [5–7] and then post-treated aerobically. While coagulation and activated carbon adsorption can be used as alternative colour removal methods [8–10], their success is rather limited for reactive dyes, due to their relatively low molecular weight, very high water solubility and low affinity for these adsorbents [3].

Recent experimental investigations have revealed that reactive dyes can be decolorised by advanced oxidation processes (AOPs) [8,11–13]. AOPs are ambient temperature processes involving the formation of hydroxyl radicals ($OH^{\bullet}$) that aggressively and almost indiscriminately attack all types of inorganic and organic pollutants found in water and wastewater [14,15]. Most of the AOPs comprise combinations of UV-light with powerful oxidizing agents such as O_3 and H_2O_2 [16]. In this regard, ozonation has been viewed as an expensive and unsafe process [17], while the major drawbacks of UV-C ($\lambda < 300$ nm)-driven treatment systems such as O_3/UV-C, H_2O_2/UV-C and Fenton/UV-C are the limited reactor configurations and high operational costs [17].

Among the AOPs, the photo-Fenton ($Fe^{2+/3+}$/H_2O_2/UV) reaction [18–21] and titanium dioxide-mediated heterogeneous photocatalytic (TiO_2/UV-A) treatment process [22–24] are capable of absorbing in the near-UV spectral region (300 nm $< \lambda <$ 400 nm) to initiate radical reactions. Their application would practically eliminate major operating costs when solar radiation is employed instead of artificial UV light.

Recently, the ferrioxalate solution that was used for decades as a chemical actinometer [25] has been applied in the photo-Fenton process, thus allowing further benefit from solar radiation [26]. In this way, the well-known Fenton's reagent leads to $OH^{\bullet}$ production [27–29]. The basic equations associated with the photolysis of Fe(III)-species and the Fenton reactions for the Fe(III)/H_2O_2/UV-A and Fe(III)$(C_2O_4)_3^{3-}$/UV-A systems are given in Eqs. (1)–(4) [30,31]:

Photolysis of Fe(III)-species:

$$Fe(III)(OH)^{2+} \xrightarrow{h\nu} Fe(II) + OH^{\bullet} \quad (1)$$

$$k = 0.0012\ s^{-1}$$

$$Fe(III)(C_2O_4)_3^{3-} \xrightarrow{h\nu} Fe(II)(C_2O_4)_2^{2-} + C_2O_4^{-\bullet} \quad (2)$$

$$k = 0.04\ s^{-1}$$

Fenton reactions:

$$Fe^{2+}H_2O_2 \rightarrow Fe^{3+} + OH^{\bullet} + OH^{-} \quad (3)$$

$$k = 53\ M^{-1}s^{-1}$$

$$Fe(II)C_2O_4 + H_2O_2 \rightarrow Fe(III)(C_2O_4)^{+} + OH^{\bullet} + OH^{-} \quad (4)$$

$$k = 3.1 \times 10^4\ M^{-1}\ s^{-1}$$

The organic complexation of Fe(III) ion not only increases the speed of photolysis but also increases the quantum yield for Fe(III)-photoreduction from 0.14 to 1.2 at 313 nm [26].

Although heterogeneous photocatalysis has been extensively studied for a wide range of organic and inorganic pollutants, its application to industrial wastewater is still rare [15,32,33]. Major drawbacks of photocatalytic processes are the need to remove the catalyst after treatment and the limited surface area of semiconductors. The process of heterogeneous catalysis involves the irradiation of TiO_2 with long-UV (UV-A)

radiation and stimulation of valence band electrons in the semiconductor by radiation. Fundamentally, excited electrons jump to the conduction band leaving holes in the valence band. Possible catalytic redox reactions with electron/hole pairs include reactions with organic and inorganic constituents present in the polluted water or electron-hole recombination. Holes react with water and/or hydroxyl ions to produce $OH^{\bullet}$ or directly oxidize pollutants, while electrons react with dissolved O_2 or other electron acceptors to form additional $OH^{\bullet}$ [24].

Both advanced oxidation processes are thought to be suitable for the degradative removal of recalcitrant organic constituents in wastewater at relatively low concentrations. In the present study, their potential for removing refractory dyes from simulated dyehouse effluents at concentrations typically found in textile dyeing and rinsing water is described and compared.

2. Materials and methods

2.1. Materials

Water used throughout the experiments was distilled and deionized (Milli-Q; Milli-pore Corp.). H_2O_2 (30%), iron(III) sulphate and potassium oxalate required for the ferrioxalate-Fenton-like reactions were Merck grade and used as received. The suppliers' elemental analyses were used in calculating reagent concentrations in reaction mixtures. P25 TiO_2 with a BET (Brunauer–Emnett–Teller) surface area of 50 m^2/g and mainly the anatase (75%) crystalline form was purchased from Degussa Corp.

2.2. Simulated dyehouse effluent

A synthetic dyehouse effluent containing five representative Procion H (monofunctional)-HE

Table 1
Chemical composition of the simulated dyehouse effluent

Dyestuff (colour index)	Company	Reactive group	Concentration (mg l^{-1})
Procion Blue HERD (Reactive Blue 160)	BASF	Bisaminochlorotriazine	6.83
Procion Crimson HEXL (ref. No. PR 3930/00)[a]	BASF	Aminochlorotriazine	40.60
Procion Yellow HE4R (Reactive Yellow 84)	BASF	Bisaminochlorotriazine	15.00
Procion Navy HEXL (ref. No. PR 3830/01)[a]	BASF	Aminochlorotriazine	86.30
Procion Yellow HEXL (Reactive Yellow 138:1)	BASF	Aminochlorotriazine	33.30
Auxiliary chemical	Function in the dyeing and/or rinsing process		Concentration (g l^{-1})
Acetic acid	Neutralization		0.79
NaCl	Transfers dyestuff to fabric		41.00
Na_2CO_3	pH buffer		13.00
NaOH	Produces covalent bonds between dyestuff and fabric		0.51
Polyether based copolymer micro-dispersion (nonionic)	Anti-creasing agent		1.20
Acyl copolymer–phosphor mixture	Sequestering agent		0.85
Alkyl phenol polyglycol ether	Detergent (washing out of unfixed dyestuff)		0.50

[a] C.I. numbers have not been allocated.

(bifunctional) (BASF AG, Germany) fiber reactive dyestuffs and their corresponding auxiliary chemicals was prepared, using a mixture of ten different reactive dye formulations most often applied to cotton fibers at a local dyehouse. According to the practical information obtained from that dyehouse, typically 20% of the reactive dyes (in their unfixed/hydrolyzed form) and 100% of the dyebath auxiliaries remain in the spent dyebath, and the dyebath effluent undergoes a 5–30-fold dilution during subsequent washing and rinsing stages. The concentrations of the reactive dyes and auxiliary chemicals selected to imitate the exhausted reactive dyebath are given in Table 1, and the characterization of the 15-fold diluted dyehouse effluent simulating the dye rinse water is shown in Table 2.

The simulated dyehouse effluent had characteristic absorption maxima at 410 nm, 556 nm, and 604 nm arising from the dyes, and an absorption band at 278 nm that is probably due to the aminochlorotriazine anchor groups. It is important to note that although the dye concentration in the simulated effluent was relatively low and hence suitable for advanced oxidative treatment, the presence of $OH^{\bullet}$ radical scavenging species (e.g. CO_3^{2-} and Cl^- ions) at significant concentrations makes this wastewater difficult to treat via advanced oxidation [34,35].

Table 2
The environmental characteristics of the 1/15-fold diluted simulated dyehouse effluent

Parameter	Value
COD (mg l^{-1})	97.70
TOC (mg l^{-1})	46.80
BOD_5 (mg l^{-1})	–[a]
AOX (mg l^{-1})	0.102
A_{280nm} (m^{-1})	41.72
A_{436nm} (m^{-1})	8.79
A_{525nm} (m^{-1})	12.95
A_{620nm} (m^{-1})	10.84
CO_3^{2-} (mg l^{-1})	490.57
Cl^- (mg/l)	1659
pH (units)	10.85

[a] Below the detection limit.

2.3. UV-A photoreactor solar simulator

The experimental set-up used in the Fenton-like and TiO_2/UV-A experiments presented schematically in Fig. 1, consisted of a UV-A light source, light homogenizer, reflector, and a photoreactor with an air sparging unit.

Phillips Cleo-R UV-A fluorescent lamps (16×40 W) were mounted in a 64×110 cm sleeve support. The front of the light source was covered with a light homogenizer (1200×600×3 mm) made of UV-A transparent ground acrylic glass, to get a more homogenous and diffuse light field. To reach a nearly homogenous light field, four reflector plates covered with aluminum foil were placed perpendicular to the light homogenizer to form a frame (840×490×200 mm) for the light. On the irradiated side of the photoreactor, an average incident photon-flux density of 22 W/m^2 ($=3.95\times10^{-3}$ Einstein m^{-2} min^{-1}) was measured using a Dr. Hönle UV-A sensitive luxmeter. The local deviation of the incident photon flux density was less than 2.5%. The UV-A photoreactor was made of a polymethylmethacrylate, PMMA (Plexiglas®, Röhm GmbH, Darmstadt) double skin sheet (SDP 16/32) that was sealed on the bottom to form seven individual UV-A transmitting rectangular tubes (510×28×12 mm each). The

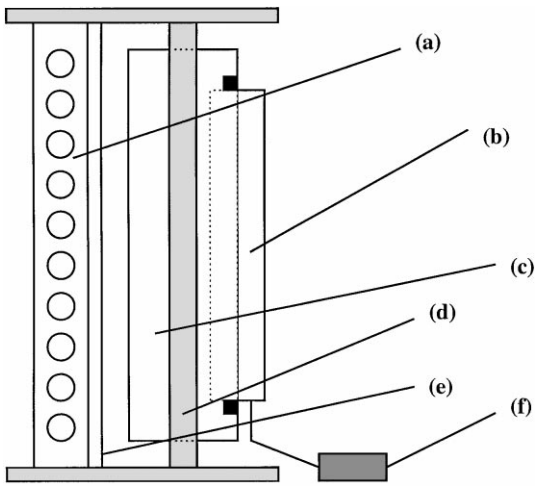

Fig. 1. Schematic of the photoreactor. (a) Light source (illuminating field), (b) photoreactor, (c) reflector, (d) supporting frame, (e) homogenizer, (f) air sparging unit.

distance between the light homogenizer and photoreactor was 190 mm. Each plexiglas tube was filled with 150 ml aliquots of the simulated dyehouse effluent, and this reaction solution had an initial irradiated surface area of 0.0125 m^2. During all experiments the photoreactor was continuously purged with air at a rate of 35 L h^{-1} to guarantee the presence of sufficient O_2 in the reacting medium (>8.5 mg l^{-1}) as well as to hold the TiO_2 synthetic dyehouse effluent mixture in suspension. The photoreactor was washed with concentrated HNO_3 solution and subsequently rinsed thoroughly with deionized water before each use to prevent iron deposition during the ferrioxalate-Fenton experiments. The lamps were allowed to burn for 30 min prior to initiating experiments, to obtain a constant light output.

2.4. Experimental procedure

For all experiments, 150 ml of simulated dyehouse effluent, prepared by diluting the simulated spent reactive dyebath at different dilution ratios (1/5–1/30), was placed inside the photoreactor and treated for one hour. Treatment conditions (e.g. oxidant, catalyst dose, and pH) were chosen according to methods from a previous study [13] and briefly described below.

2.4.1. Fenton-like reactions

For the Fenton-like experiments, the pH of the simulated dyehouse effluent was adjusted to 2.8 with H_2SO_4 (97%). Ferrioxalate was formed in the reaction mixture immediately prior to initiating the experiments. It was prepared from a solution containing a 1:3 molar ratio of Fe(III) sulphate (0.2 mM; with 0.4 mM Fe^{3+} ions) and potassium oxalate (1.2 mM) to ensure that all introduced Fe(III) was complexed with a significant fraction of oxalate ions. The pH of the resultant ferrioxalate solution was 2.60–2.65 and taken as the initial reaction pH.

The Fenton-like reactions were initiated by the introduction of 5 mM H_2O_2 (30%), giving a 1:12.5 molar ratio with respect to Fe(III) ions. The Fenton-like oxidation was stopped by adjusting the pH of the samples to 7.0–7.5 with NaOH stock solution (6 N) giving Fe(III)-floc formation. Precipitated Fe(III)-flocs were removed by centrifuging (Heraeus Sepatech Labofuge) for 40 min at 4000 rpm.

2.4.2. TiO_2/UV-A experiments

Before the photocatalytic experiments were initiated, the pH of the dyehouse effluent was adjusted to 7.0 using H_2SO_4, and 1 g/l TiO_2 powder was added. The TiO_2 slurries were sonicated for 15–20 min to obtain a homogeneous TiO_2-sample suspension. TOC and absorbance measurements confirmed that no dye degradation occurred during sonication. No significant immediate adsorption of the dyes on the catalyst surface was observed at pH = 7 in the present study, based on TOC and absorbance measurements before and after TiO_2 addition. After sample withdrawal, TiO_2 was separated by centrifuging the sample suspensions, as described for the Fenton-like reactions.

2.5. Sample analyses

For analyses, 10 ml-samples were taken periodically from the photoreactor top and pretreated as explained in Sections 2.4.1. and 2.4.2. To examine the progress of dye degradation, absorbance values were measured spectrophotometrically at four different wavelengths (620, 525, 436 and 280 nm) during the different treatment processes. The first three wavelengths were chosen because they are used in advanced treatment methods for textile wastewater discharge criteria in EU countries such as Germany [36]. Similarly, the absorption band at 280 nm was employed to assess optical densities in the UV spectral region.

UV-visible absorption spectra were determined using a Perkin–Elmer Lambda 17 spectrophotometer. TOC was analyzed using a Shimadzu TC-5000 analyzer and residual (unreacted) H_2O_2 concentration in the treated samples was determined using the molybdate-catalyzed iodometric titration procedure [37].

2.6. Kinetic evaluation of reactive dyestuff degradation with respect to initial dyehouse effluent dilution ratio

To examine the progress of decolourization, absorbance values were determined spectrophotometrically at 620, 525, and 436 nm and at five effluent dilution ratios (1/5, 1/10, 1/15, 1/20 and 1/30). For the investigated AOPs, decolourization followed first-order reaction kinetics at all effluent dilution ratios. Thus the use of a simple pseudo-first order rate expression [Eq. (5)] was appropriate:

$$-\ln(A/A_i) = k_{app} \times t \quad (5)$$

where k_{app} is the pseudo-first order decolourization rate constant (in min^{-1}) and A is the absorbance at the wavelengths employed (in m^{-1}).

In the case of heterogeneous photocatalytic treatments the effects of initial dyehouse effluent strength as a function of the dilution ratio of the exhausted synthetic dyebath were evaluated using the Langmuir–Hinshelwood (L–H) approach that is commonly applied to photocatalytic oxidation processes [38,39]. Eq. (6) is used to provide an approximation over a wide range of pollutant concentrations:

$$-\ln(A/A_i) = k_r \times K \times t = k_{app} \times t \quad (6)$$

where k_r is the reaction rate constant (in m^{-1} min^{-1}), K is the equilibrium adsorption constant (in m) and k_{app} is the apparent first-order reaction rate constant (in min^{-1}). In the case that gave decreasing k_{app} values with increasing initial absorbance (A_I) of the dyehouse effluent, the overall decolourization rate was the sum of zero- and first-order decolourization [40]:

$$\ln(A/A_i) + K(A_i - A) = k_r \times K \times t \quad (7)$$

Using the L–H kinetic model in tandem with Eq. (7), a linear plot of $t_{1/2}$ versus A_i is obtained:

$$t_{1/2} = 0.693/(k_r \times K) + 0.5A_i/k_r \quad (8)$$

3. Results and discussion

3.1. Photolytic decomposition of ferrioxalate

Since the addition of 1.2 mM ferrioxalate at the beginning of the Fenton-like reaction contributed to the organic load of the dyehouse effluent ($TOC_{ferrioxalate} = 29$ mg/l), its fate in the reaction medium merits special consideration. Fig. 2 illustrates UV-A-light induced TOC abatement of 1.2 mM ferrioxalate solution in the absence and presence of H_2O_2 as a function of irradiation time. Both sets of data reflect rapid mineralization of oxalate with pseudo-first order kinetics. When H_2O_2 was introduced, ferrioxalate completely mineralized within three minutes, nearly five times faster than without H_2O_2. As a consequence, oxalate addition did not interfere with TOC measurements after a few minutes of exposure to UV-A light.

3.2. Process efficiency of different Fenton-like reactions

To demonstrate the superiority of the ferrioxalate-photo-Fenton process over the conventional inorganic photo-Fenton reaction, the treatment efficiencies of different Fenton-like reaction types were compared in terms of selected process parameters. Since H_2O_2 can also act as an effective $OH^{\bullet}$ scavenger when used at high doses, a control experiment was conducted to determine whether a two-step H_2O_2 addition would be a beneficial

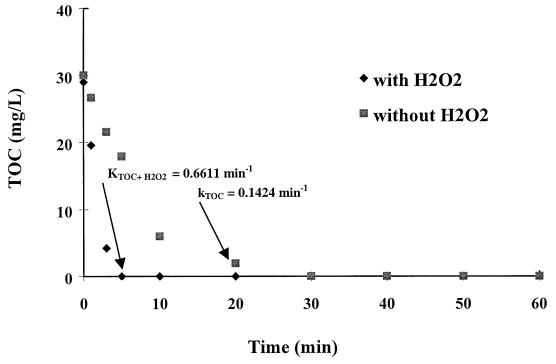

Fig. 2. TOC abatement during photocatalytic decomposition of ferrioxalate solution in the absence and presence of H_2O_2.

wastewater treatment process. Half of the H_2O_2 (2.5 mM) was added at the beginning of the reaction and the remainder was added after a 10-min irradiation period.

Apparent first-order decolourization rate constants for the reduction of absorbance at 525 nm and the % TOC and UV_{280nm} removal rates after different 1-h Fenton-like treatments are depicted in Fig. 3.

The data in Fig. 3 show that the highest overall % TOC reduction was observed via Fe(III)-oxalate-Fenton/UV-A oxidation (Fenton type A). It is clear that Fe(III)-oxalate UV-A photolysis in the absence of H_2O_2 (Fenton type C) gave an 18 times lower decolourization rate constant than the Fe(III)-oxalate-Fenton/UV-A process (Fenton type A) and an overall UV_{280nm} reduction rate of 13%. The data also clearly revealed that the two-step H_2O_2 addition process (Fenton type D) was not beneficial, since dye degradation and hence oxidant consumption were appreciably higher when all of the H_2O_2 was added at the beginning of the AOP. The lower quantum yield associated with Fe(III)/H_2O_2/UV-A oxidation (Fenton type B) resulted in an appreciably reduced treatment efficiency, indicating that the photoreduction of Fe(III)-oxalate complexes produced a higher level of $OH^\bullet$ radicals than the photolysis of ordinary Fe(III) salts [26]. In the case of the dark Fe(III)-oxalate-Fenton reaction (Fenton type E), no degradation took place since these Fenton-like conditions do not produce $OH^\bullet$ [28]. This means that day light-induced $OH^\bullet$ formation was quite slow and inefficient compared to the UV-A-induced Fenton-like processes (Fenton types A, B and D).

3.3. Correlation between H_2O_2 consumption and UV_{280nm} removal

Data for residual H_2O_2 concentration and parallel UV_{280nm} removal as a function of advanced oxidation time for 1/15 diluted reactive dye wastewater, under various Fenton-like conditions are presented in Fig. 4. During Fe(III)-oxalate-Fenton/UV-A oxidation, 67% of the initially introduced H_2O_2 was consumed within the first 10 min of this treatment and practically all (95%) of the oxidant employed was depleted after one hour treatment time (Fig. 4a). However, during the Fe(III)-Fenton/UV-A process, 40% of the H_2O_2 employed remained in the reaction medium after one hour. In the Fe(III)-oxalate-Fenton/UV-A process that involved the two-step H_2O_2 addition, only 48% of the second portion of H_2O_2 was consumed during the same treatment period. Almost no H_2O_2 consumption occurred during the dark control experiment (Fenton type E),

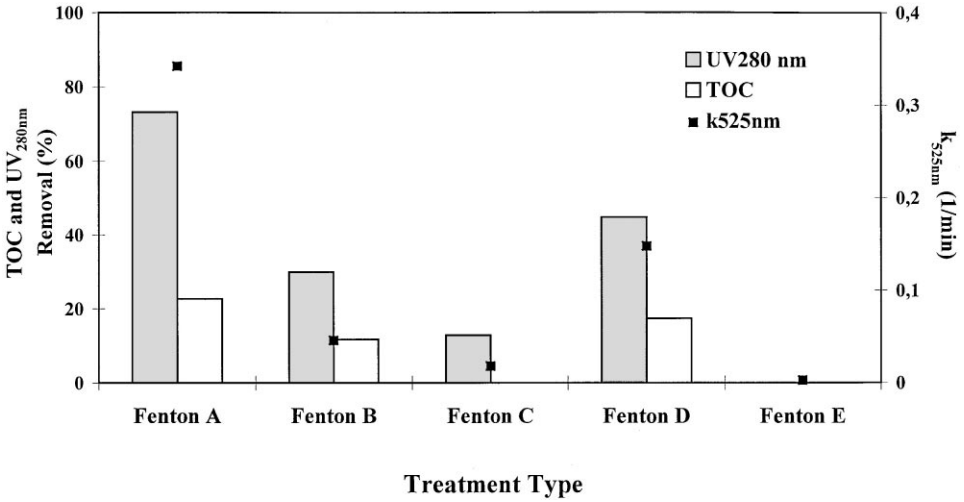

Fig. 3. Overall per cent UV_{280nm}, TOC removal and k_{525nm} values obtained for 1-h treatment via different Fenton-like reactions. Fenton A–E types refer to varying Fenton-like processes (cf. Section 3.1).

revealing that since the photo-reduction of Fe(III) to Fe(II) does not take place in the absence of UV light, there was no mechanism for H_2O_2 depletion via reactions (3) and (4). The results obtained from Fe(III)-oxalate-Fenton/UV-A treatment and control experiments indicated the presence of a linear correlation ($R^2 = 0.94$) between H_2O_2 consumption and UV_{280nm} degradation. Fig. 4 shows that an increase in UV_{280nm} values took place within the first minute of all advanced oxidation processes, probably due to the formation of soluble ferriorgano and ferrihydroxycomplexes that decomposed quickly thereafter in the presence of UV-A light and H_2O_2. This is consistent with the formation of strongly UV-A absorbing unstable species in all Fenton-like experiments directly after Fe(III) addition [41,42].

Although ferriorgano complex formation was observed in all of the present Fenton-like reactions,

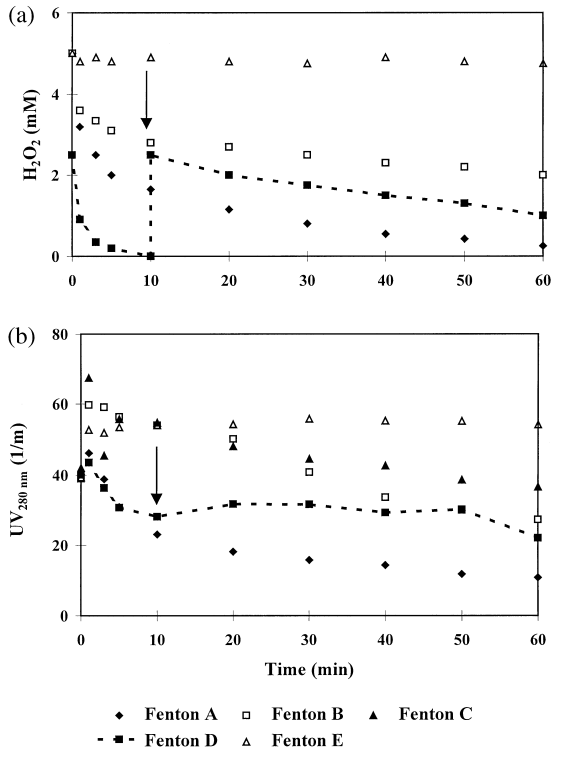

Fig. 4. H_2O_2 consumption (a) and UV_{280nm} abatement (b) obtained for 1-h treatment via different Fenton-like reactions. Fenton A–E types refer to varying Fenton-like processes (cf. Section 3.1). The arrow indicates the time of H_2O_2 addition.

the major reason for the marginally higher reaction rate of the ferrioxalate/H_2O_2/UV-A process is the fact that the ferrioxalate-Fenton/UV-A process is more effective for wastewater containing polyaromatic compounds such as dyes [26]. These compounds would normally compete with Fe(III)-ions for UV-light (H_2O_2 only photolyses below 300 nm), leading to the very slow destruction rate of parent molecules that was also observed in the present study. Ferrioxalate on the other hand absorbs light more effectively in the 250–500 nm region; thus interferences by these contaminants still leaves 350–450 nm light available for absorption by ferrioxalate [26].

3.4. Decolourization kinetics of Fenton-like processes

A series of experiments was conducted at five different dyehouse effluent concentrations (dilution ratios of 1/5, 1/10, 1/15, 1/20 and 1/30) to assess the impact of solute concentration on the decolourization rate constant. Fig. 5 shows plots of $t_{1/2}$ (decolourization half-life) versus A_i (initial absorbance) at 436, 525 and 620 nm. It is clear that a linear relationship between $t_{1/2}$ and A_i was found. Generally, the absorption bands at longer wavelengths were removed much faster, with the blue colour disappearing somewhat faster than red and yellow. A five- (436 nm), six- (525 nm) and eight-fold (620 nm) increase in A_i resulted in an approximately four- (436 nm) and three-fold (525 nm–620 nm) increase in the decolourization rate constant (k_{app}).

3.5. Process efficiency of TiO_2-mediated photocatalytic treatments

During all photocatalytic experiments the pH of the reaction medium did not change significantly from the initial pH7 value. The synthetic effluent contained appreciable amounts of CO_3^{2-} (Table 2), creating an HCO_3^-/CO_3^{2-} equilibrium that served as an effective pH7 buffer.

Fig. 6 provides k_{525nm} values, overall % UV_{280nm} and TOC removal efficiencies as a function of photocatalytic treatment time for the TiO_2/UV-A reaction, and data from control experiments

involving 1/15 diluted reactive dye wastewater. It is clear from these data that the decolourization rate constant was three times lower in the TiO_2/UV-A process versus the Fe(III)-oxalate-Fenton/UV-A process. Similarly, Spaceck et al. [43] found that the decomposition of phenolic compounds and their intermediates by the photo-Fenton process was much higher than by TiO_2-mediated photocatalytic degradation. In that study, a higher level of $OH^{\bullet}$ radical formation also seemed to be the primary reason for the higher degradation rates in Fenton-like process.

The overall UV_{280nm} and TOC removal efficiencies were 86 and 17%, respectively, after a 1-h photocatalytic treatment and, thus, was slightly better at removing aromaticity than the Fe(III)-oxalate-Fenton/UV-A process (73% UV_{280nm} and 23% TOC removal). It was also found that the TOC kinetics were zero-order for photocatalytic treatments and the other investigated treatment processes. Adsorption on the photocatalyst surface was not observed under dark conditions at pH7, where TiO_2 carries a negative charge ($TiO_{2zpc} = 6.3$) [24], and thus the anionic dyes in the simulated dyehouse effluent were electrostatically repelled. Since certain reactive dyes possess good photochemical stability, it was not surprising that degradation by direct UV-A treatment in the absence of semiconductor did not occur.

As found with the photo-Fenton reactions, a decrease in UV_{280nm} values (Fig. 7) started after a 10-min photocatalytic treatment, indicating fragmentation of the aromatic molecules into smaller, colorless compounds following the interactions between OH radicals and the parent dye structures.

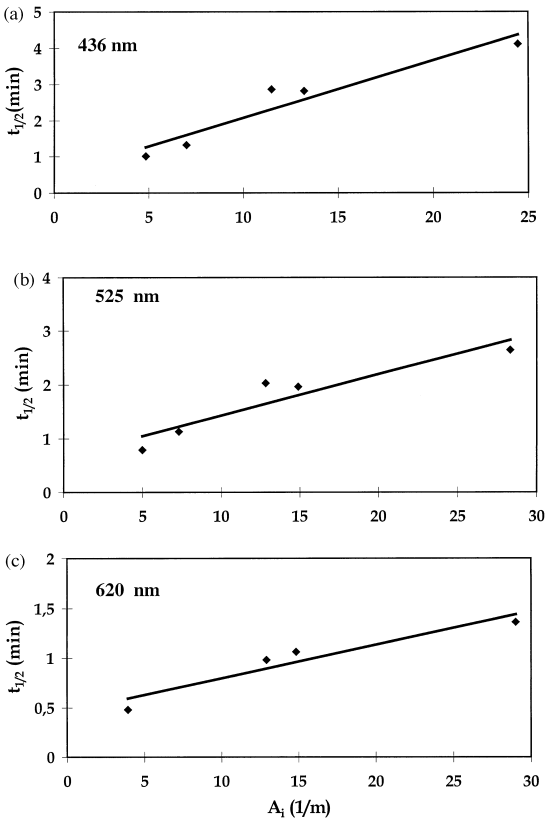

Fig. 5. Plots of $t_{1/2}$ versus A_i at 436 nm (a), 525 nm (b) and 620 nm (c) wavelengths for ferrioxalate/H_2O_2/UV-A treatment.

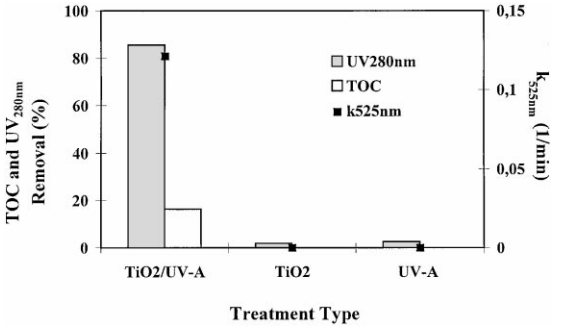

Fig. 6. Overall per cent UV_{280nm}, TOC removal and k_{525nm} values obtained for 1 h-treatment with TiO_2/UV-A, TiO_2 and UV-A only.

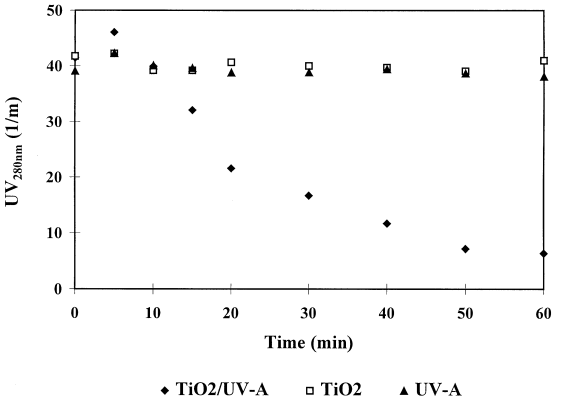

Fig. 7. UV_{280nm} abatement as a function of photocatalytic treatment time for TiO_2/UV-A, TiO_2 and UV-A only.

3.6. Decolourization kinetics as a function of initial dyehouse effluent strength for the TiO_2/UV-A treatment process

For the TiO_2/UV-A process, the empirical L–H kinetic model was employed to describe the photocatalytic decolourization process. This model assumes that photocatalytic treatments involve complex processes in which pollutants are first adsorbed and subsequently degraded on the photocatalyst surface. Plots of $t_{1/2}$s versus A_i values are displayed in Fig. 8.

The kinetic equations given in Fig. 8(a–c) provide the K and k_r values of the L–H kinetic model that were determined from the intercept and slope of the straight lines, respectively.

Pseudo-first order rate constants for decolourization decreased with increasing dyehouse effluent strength, due to the combined effects of increased dye concentration and decreased optical density of the effluent. Similar observations were made in a previous study that pertained to the ozonation of spent reactive dyebath effluents [44]. Furthermore, photocatalytic decolourization rate constants (k_r values) increased at higher wavelengths and a parallel slight decrease in adsorption constants (K values) was observed. As a consequence of the neutral pH, the calculated K values were relatively low, and photocatalytic degradation rather than adsorption was responsible for the observed colour removal. From K and k_r constants in which $K << k_r$, it is apparent that light-induced adsorption is the rate limiting step of photocatalytic decolourization.

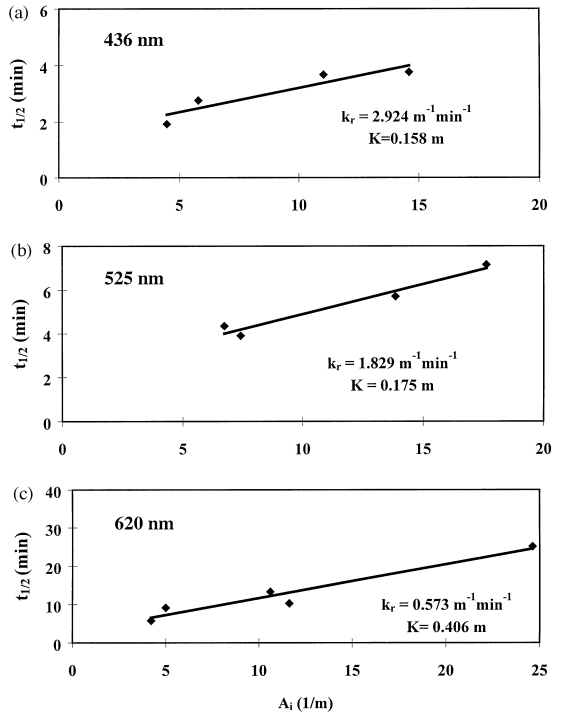

Fig. 8. Plots of $t_{1/2}$ versus A_i at 436 nm (a), 525 nm (b) and 620 nm (c) for the TiO_2/UV-A treatment process.

4. Conclusions

It has been found that simulated reactive dyewastewater can be effectively treated by homogeneous Fe(III)-oxalate-Fenton/UV-A and heterogeneous TiO_2/UV-A reactions in a novel photoreactor under O_2-saturated conditions at pH = 2.6 and 7.0, respectively. It is also clear that:

1. The more dilute the initial effluent the faster the dye degradation.
2. The empirical L–H kinetic model is applicable to the photocatalytic decolourization reactive dyes at various concentrations in dyehouse effluents.
3. Decolourization is faster using ferrioxalate-Fenton/UV-A oxidation, whereas the TiO_2/UV-A process is slightly better in overall UV_{280nm} removal. The best TOC abatement occurs after a one hour treatment.
4. For the Fenton-like reactions, a positive correlation exists between the extent of UV_{280nm} removal rate (dye modification/degradation of) and H_2O_2 consumption.
5. No dye degradation is observed in the absence of UV-A irradiation.
6. The cost of the pH-adjustment (to pH7) ultimately determines whether an improvement in treatment efficiency by pH-regulation is economical.

Acknowledgements

This experimental work was performed under the auspices of Bogaziçi University Research Project Nr. 98Y03. Idil Arslan wishes to express her thanks to TÜBITAK BAYG for the NATO A2 scholarship and to ISFH (Institut für Solarenergieforschung GmbH), Hannover, Germany), where the study was conducted.

References

[1] Reife A, Freeman HS. Environmental chemistry of dyes and pigments. Canada: John Wiley and Sons Inc., 1996.
[2] Easton JR. The problem of colour, the dye maker's view. In: Cooper P, editor. Colour in dyehouse effluent. Oxford. The Society of Dyers and Colourists, Alden Press.
[3] Reife A. Dyes, environmental. In: Dyes, environmental chemistry. Kirk–Othmer Encyclopedia of Chemical Technology. 4th ed., vol. 8. John Wiley and Sons, New York, 1993. p. 753–84.
[4] Pagga U, Brown D. The degradation of dyestuffs part II: behavior of dyestuffs in aerobic biodegradation tests. Chemosphere 1986;15:479–91.
[5] Carliell CM, Barclay SJ, Naidoo N, Buckley CA, Mulholland DA, Senior E. Microbial decolourisation of a reactive azo dye under anaerobic conditions. Water SA 1981;21:61–9.
[6] Razo-Flores E, Luitjen M, Donlon B, Lettinga G, Field J. Biodegradation of selected azo dyes under methanogenic conditions. Wat Sci Technol 1997;36:65–72.
[7] Brown D, Hamburger B. The degradation of dyestuff: Part III – investigation of their ultimate degradability. Chemosphere 1987;16:1539–53.
[8] Bahorsky MS. Textiles Wat Environ Res 1997;69:658–64.
[9] Grau P. Textile industry wastewaters treatment. Wat Sci Tech 1991;24:97–103.
[10] Vandevivere PC, Bianchi R, Verstraete W. Treatment and reuse of wastewater from the textile wet-processing industry: review and emerging technologies. J Chem Technol Biotechnol 1998;72:289–302.
[11] Marechal AM, Slokar YM, Taufer T. Decoloration of chlorotriazine reactive azo dyes with H_2O_2/UV. Dyes and Pigments 1997;33:281–98.
[12] Solzhenko EG, Soboleva NM, Goncharuk VV. Decolourization of azo dye solutions by Fenton's oxidation. Wat Res 1995;29:2206–10.
[13] Arslan I, Balcioglu IA. Degradation of commercial reactive dyestuffs by heterogeneous and homogeneous advanced oxidation processes: a comparative study. Dyes and Pigments 1999;43:95–108.
[14] Bolton JR, Cater SR. In: Helz G, Zepp R, Crisby D, editors. Surface and aquatic environmental photochemistry. Boca Raton, FL: CRC Press, 1994. p. 467–90.
[15] Legrini O, Oliveros E, Braun AM. Photochemical processes for water treatment. Chem Rev 1993;93:671–98.
[16] Glaze WH, Kang JW, Chapin DH. The chemistry of water treatment processes involving ozone, hydrogen peroxide and ultraviolet radiation. Oz Sci & Engrg 1987;9:335–52.
[17] The AOT handbook. Calgon Carbon Oxidation Technologies, Markham, Ontario, 1995.
[18] Safarzadeh-Amiri A, Bolton JR, Cater SR. The use of iron in advanced oxidation processes. J Adv Oxid Technol 1996;1:18–26.
[19] Ruppert G, Bauer R. The photo-Fenton reaction — an effective photochemical wastewater treatment process. J Photochem Photobiol A: Chem 1993;73:75–8.
[20] Zepp RG, Hoigné J. Hydroxyl radical formation in aqueous reactions (pH 3–8) of iron(II) with hydrogen peroxide. Environ Sci Technol 1992;26:313–9.
[21] Pignatello JJ. Dark and photoassisted Fe^{3+}-catalyzed degradation of chlorophenoxy herbicides by hydrogen peroxide. Environ Sci Technol 1992;26:944–51.
[22] Ollis DF, Pelizzetti E, Serpone N. Heterogeneous photocatalysis in the environment: application to water purification. In: Serpone NN, Pelizzetti E, editors. Photocatalysis: fundamentals and applications. New York: John Wiley and Sons, 1989. p. 603–37.
[23] Pichat P, Guillard C, Maillard C, Amalric L, D'Oliveira J. Photocatalytic destruction of aromatic pollutants; intermediates; properties–degradability correlation; effects of inorganic ions and TiO_2 surface area, comparison with H_2O_2 processes. In: Ollis DF, Al-Ekabi H., editors. Photocatalytic purification and treatment of water and air. Amsterdam: Elsevier, 1993. p. 207–23.
[24] Bahnemann D, Cunningham J, Fox MA, Pelizetti E, Pichat P, Serpone N. Photocatalytic treatment of waters. In: Helz G, Zepp R, Crosby D, editors. Aquatic and surface photochemistry. Boca Raton: Lewis Publishers, 1994. p. 261–316.
[25] Hatchard CG, Parker CA. A new sensitive chemical actinometer. II. Potassium ferrioxalate as a standard chemical actinometer. Proc R Soc London 1956;A235: 518–536.
[26] Safarzadeh-Amiri A, Bolton JR, Cater S. Ferrioxalate-mediated photodegradation of organic pollutants in contaminated water. Wat Res 1997;31:787–98.
[27] Fenton HJH. Oxidation of tartaric acid in presence of iron. J Chem Soc 1894;65:899.
[28] Walling C. Fenton's reagent revisited. Acc Chem Res 1975;8:125–31.
[29] Barbeni M, Minero C, Pelizzetti E, Borgarello E, Serpone N. Chemical degradation of chlorophenols with Fenton's reagent. Chemosphere 1987;16:2225–37.
[30] Balzani V, Carassitti V. Photochemistry of coordination compounds. Academic Press, London, 1970. pp. 145–92 [chapter 10].
[31] Bolton JR, Ravel M, Cater SR, Safarzadeh-Amiri A. Homogeneous solar photodegradation of contaminants in water. Proceedings of ASME, 1996. pp. 53–60.

[32] Balcioglu Akmehmet I, Arslan I. Treatment of textile wastewater by heterogeneous photocatalytic oxidation processes. Environ Technol 1997;18:1053–9.
[33] Balcioglu Akmehmet I, Arslan I. Application of photocatalytic oxidation treatment to pretreated and raw effluents from the Kraft bleaching process and textile industry. Env Poll 1998;103:261–8.
[34] Schmelling DC, Gray K, Kamat PV. The influence of solution matrix on the photocatalytic degradation of TNT in TiO_2 slurries. Wat Res 1997;31:439–1447.
[35] Buxton GV, Greenstock CL, Helman WP, Ross AB. Critical review of rate constants for reaction of hydrated electrons, hydrogen atoms and hydroxyl radicals ($OH^{\bullet}$/$O^{-\bullet}$) in aqueous solution. J Phys Chem Ref Data 1988;17:513–886.
[36] Schulze-Rettmer R. Das Problem der Restfaerbung des Abwassers von Faerbereien. Textilveredlung 1996;31:13–18.
[37] Horwitz W., editor. Official methods of analysis 13th ed. Washington: Association of Official Analytical Chemists, 1980.
[38] Ollis DF. Contaminant degradation in water. Environ Sci Technol 1985;19:480–4.
[39] Mattthews RW. Purification of water with near-UV illuminated suspensions of titanium dioxide. Wat Res 1990;24:653–60.
[40] Al-Ekabi H, Serpone N. Kinetic studies in heterogeneous photocatalysis. 1. Photocatalytic degradation of chlorinated phenols in aerated solutions over TiO_2 supported on a glass matrix. J Phys Chem 1988;92:5726–31.
[41] Faust BC, Hoigné J. Photolysis of Fe(III)-hydroxy complexes as sources of OH radicals in clouds, fog and rain. Atmos Environ 1990;24A:79–89.
[42] Faust BC, Zepp RG. Photochemistry of iron(III)-polycarboxylate complexes: roles in the chemistry of atmospheric and surface waters. Environ Sci Technol 1993;27:2517–2522.
[43] Spaceck W, Bauer R, Heisler G. Heterogeneous and homogeneous wastewater treatment–comparison between photodegradation with TiO_2 and the photo-Fenton reaction. Chemosphere 1995;30:477–84.
[44] Arslan I, Balcioglu Akmehmet I. Effect of common reactive dye auxiliaries on the ozonation of vinylsulphone and aminochlorotriazine containing dyehouse effluent. Desalination 2000;130:61–71.